J. Fluid Mech. (2006), *vol.* 550, *pp.* 1–25.
doi:10.1017/S0022112005007676 Printed in the United Kingdom

A three-phase mixture theory for particle size segregation in shallow granular free-surface flows

By A. R. THORNTON[1], J. M. N. T. GRAY[1] AND A. J. HOGG[2]

[1]School of Mathematics, University of Manchester, Manchester M13 9PL, UK

[2]Centre for Environmental & Geophysical Flows, School of Mathematics, University of Bristol, University Walk, Bristol BS8 1TW, UK

(Received 5 October 2004 and in revised form 15 July 2005)

Particle-size segregation within granular materials is of great technological significance yet it is still very poorly understood. There are several causes of segregation, but this paper focuses on kinetic sieving which is the dominant mechanism in dense gravity-driven shallow free-surface flows, or, granular avalanches. The segregation model is derived from a three-phase mixture theory composed of large particles, small particles and a passive interstitial fluid. Steady-state solutions are constructed for a normally graded inflow in a steady uniform flow field. This problem is of fundamental interest, because it shows how an unstably stratified layer readjusts into a stable configuration. Expansion fans and concentration shocks are generated and sufficiently far downstream inversely graded segregated layers form, with the larger particles overlying the finer ones. This a good approximation for segregation in flows with weak diffusive remixing. The distance for complete segregation to occur is shown to increase with rising fluid density and tends to infinity as its density approaches that of the grains. If the particles are buoyant then the initial configuration is stable. An exact time-dependent two-dimensional solution is constructed for plug flow, which exploits the uncoupling of material columns of grains in the absence of shear. This yields insight into the nature of more complex numerical solutions for strong shear, which are computed with a high-resolution shock-capturing numerical scheme.

1. Introduction

Many industrial processes use materials in a granular form, as they are easy to produce and store. Often grains with dissimilar properties need to be mixed together or separated from one another and a variety of devices have been designed to do this. Rotating drums and blenders (e.g. Metcalfe *et al.* 1995; Shinbrot, Alexander & Muzzio 1999; Hill *et al.* 1999; Gray 2001) are often used in the pharmaceutical and food industry, while rotary kilns and inclined rotating cylinders (e.g. Davidson *et al.* 2000; Spurling, Davidson & Scott 2001) are favoured by chemical engineers for sintering, calcination, humidification, oxidation, drying, mixing, induration, reducing, gas–solid reaction, incineration, heating, cooling and cement production, because they allow continuous feed. These fields represent a substantial worldwide financial turnover. Sales in powdered metals alone exceed 6 billion euros in Europe and another $5 billion in North America. Often the segregation that takes place within these processes is unintended and unwanted. The effects can range from tablets with too much, or too little, of an active ingredient (Williams 1968; Staniforth 1982), to

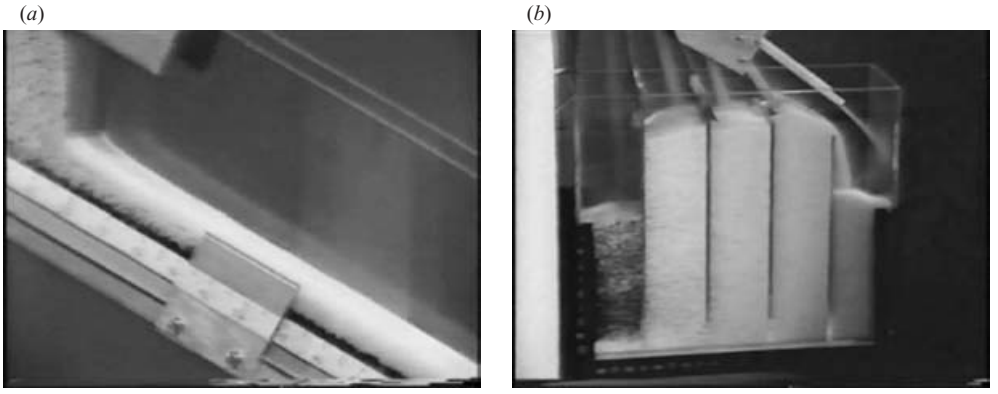

FIGURE 1. Two stills taken from Savage & Lun's (1988) experiments showing that very sharp segregation occurs when there is low diffusive remixing. The large (white) and small (black) particles are homogeneously mixed and flow out of a hopper. They rapidly segregate into inversely graded layers (*a*) with a sharp concentration jump between them. Savage & Lun (1988) used a series of splitter plates to take samples of the particle concentration at different levels in the flow (*b*). These show that the there are very high concentrations of large particles in the upper layers and very large concentrations of small particles in the lower layers.

less effective washing detergents. Despite its importance our physical understanding of segregation is limited and in most practical situations engineers have to rely on purely empirical guidelines (Johanson 1978).

There are a number of mechanisms for segregation (Bridgewater 1976; Cooke, Stephens & Bridgewater 1976), but this paper focuses on particle-size segregation by *kinetic sieving* (Middleton & Hampton 1976), which is the dominant mechanism in dense gravity-driven free-surface flows or granular avalanches (Bridgewater 1976; Savage & Lun 1988). The process is simple. During an avalanche there are small fluctuations in the void space between the particles. As a void opens up beneath a layer of particles, the small particles are more likely to fall into it, because they are more likely to fit into the available space than the large grains. The fines therefore tend to drop down towards the base of the flow, and force imbalances drive a reverse flow of large particles towards the free-surface by a process known as *squeeze expulsion*. In dry frictional flows kinetic sieving is so efficient that segregated *inversely graded* layers rapidly develop, with very high concentrations of coarse particles separated by a sharp concentration jump from very high concentrations of fines below. Figure 1 shows two photos from Savage & Lun's (1988) experiments. A mixture of grains enters from the hopper on the left and flows down chute. Very rapidly the particles segregate out to form inversely graded layers with a very sharp concentration jump between them as can be seen at the bottom of figure 1(*a*). The segregation was so sharp, in fact, that this motivated Savage & Lun to treat the interface as a shock. This sharp transition in the particle concentration was confirmed by detailed concentration data that was obtained using an array of splitter plates to bin samples from different layers in the flow (figure 1*b*). Similar experiments have also been performed by Vallance & Savage (2000) and they also observed very sharp segregation shocks. As the flows become more energetic diffusive remixing competes with the kinetic sieving mechanism to produce a smoothly varying inversely graded layer (Dolgunin & Ulokov 1995; Jenkins & Yoon 2001). Distributed inversely, or *reverse*, graded deposits are often left by large-scale geophysical granular flows such as rockfalls, lahars, debris

flows and pyroclastic flows (Vallance 2000; Iverson & Vallance 2001), which allows geologists to distinguish them from *normally* graded deposits formed as particles settle out of suspension in quiescent water. In this paper we investigate the weak diffusive-remixing limit, where the rapid transitions between regions of high and low concentrations of small/large particles observed in experiments (Savage & Lun 1988; Vallance & Savage 2000) are replaced by concentration jumps or shocks.

Although considerable theoretical attention has been focused on particle-size segregation in energetic collisional flows (e.g. Jenkins & Mancini 1987; Jenkins 1998; Jenkins & Yoon 2001) there has been very little analysis of the kinetic sieving process in slower dense free-surface flows. The first theory was derived by Savage & Lun (1988) using statistical mechanics and information entropy ideas. Their model was able to predict the steady-state particle-size distribution in a steady uniform flow and the results compared well with an extensive series of experiments. One disadvantage of Savage & Lun's (1988) model was that there was no explicit dependence of the segregation velocities on gravity, even though kinetic sieving is a fundamentally gravity-driven process. Gray & Thornton (2005) used individual constituent mass and momentum balances in the framework of a binary mixture theory to formulate a model for kinetic sieving, which provided a natural way of introducing gravity. The key idea behind the model was that as the small particles percolated down through the matrix, the large particles had to support a greater proportion of the overburden pressure. This suggested a nonlinear partial-intrinsic pressure scaling, which when combined with a linear frictional resistance to percolation, led to a very simple mathematical model for kinetic sieving. Gray & Thornton's (2005) model consists of a single hyperbolic equation for the volume fraction of small particles, which is able to predict the complete three-dimensional temporal and spatial evolution of the particle-size distribution in a prescribed incompressible flow field. This fits naturally into the structure for models of shallow granular free-surface flows (e.g. Grigorian, Eglit & Lakimov 1967; Kulikovskii & Eglit 1973; Eglit 1983; Savage & Hutter 1989; Gray, Wieland & Hutter 1999; Gray, Tai & Noelle 2003), which all assume that the material is incompressible and the pressure is lithostatic. It is therefore possible to envisage coupled models to explain some of the complex feedback mechanisms that particle-size segregation can have on both geophysical flows (Pouliquen, Delour & Savage 1997; Pouliquen & Vallance 1999; Calder, Sparks & Gardeweg 2000; Iverson 2003) and in industrial rotating drums and kilns (Zik *et al.* 1994; Hill & Kakalios 1995).

In this paper a three-constituent mixture theory is used to extend the kinetic-sieving model of Gray & Thornton (2005) by including a passive fluid in the interstitial pore space between the large and small particles. This extends the model to water-saturated debris flows (e.g. Iverson 1997, 2003; Iverson & Denlinger 2001) and shows that for dense fluids significant buoyancy forces can be exerted on the particles, which can slow, prevent or reverse the segregation.

2. Three-constituent segregation model

2.1. *Mixture framework*

The granular material is assumed to be composed of a bi-disperse mixture of large and small particles, whose interstitial pore space is filled with a passive fluid. A three-constituent continuum mixture theory (e.g. Truesdell 1984; Morland 1992) is therefore used to model the system, which assumes that every point is simultaneously occupied by all three phases. This allows overlapping partial density ρ^{ν}, partial velocity $\boldsymbol{u}^{\nu}$ and

partial pressure p^ν fields to be defined for each constituent ν. The large particles will be denoted by the superscript 'l', the small particles by 's' and the passive fluid by 'a'. Each constituent must satisfy individual conservation laws for mass

$$\frac{\partial \rho^\nu}{\partial t} + \nabla \cdot (\rho^\nu \boldsymbol{u}^\nu) = 0, \tag{2.1}$$

and momentum

$$\frac{\partial}{\partial t}(\rho^\nu \boldsymbol{u}^\nu) + \nabla \cdot (\rho^\nu \boldsymbol{u}^\nu \otimes \boldsymbol{u}^\nu) = -\nabla p^\nu + \rho^\nu \boldsymbol{g} + \boldsymbol{\beta}^\nu, \tag{2.2}$$

where $\otimes$ is the dyadic product and $\boldsymbol{g}$ is the acceleration due to gravity. The interaction force $\boldsymbol{\beta}^\nu$ is the force applied on constituent ν by the other components. As these forces are internal to the system, Newton's third law implies that they must sum to zero

$$\boldsymbol{\beta}^l + \boldsymbol{\beta}^s + \boldsymbol{\beta}^a = \boldsymbol{0}. \tag{2.3}$$

The bulk density ρ and bulk pressure p are defined by the sum of the partial quantities over all constituents

$$\rho = \rho^l + \rho^s + \rho^a, \qquad p = p^l + p^s + p^a. \tag{2.4}$$

Each constituent occupies a volume fraction Φ^ν per unit mixture volume, and by definition these sum to unity

$$\Phi^l + \Phi^s + \Phi^a = 1. \tag{2.5}$$

It is useful to work with the volume fraction of large and small particles per unit granular volume rather than per unit mixture volume. Since, the volume fraction of grains per unit mixture is

$$\Phi^g = \Phi^l + \Phi^s, \tag{2.6}$$

the volume fractions of large and small particles per unit granular volume are

$$\phi^\mu = \Phi^\mu / \Phi^g, \qquad \mu = l, s, \tag{2.7}$$

which also sum to unity

$$\phi^l + \phi^s = 1. \tag{2.8}$$

A key element of mixture theory is the relationship between the partial and intrinsic, or physical, variables, which are measurable. Morland (1992) showed that the partial velocity and density are related to their intrinsic counterparts by

$$\boldsymbol{u}^\nu = \boldsymbol{u}^{\nu *} \quad \text{and} \quad \rho^\nu = \Phi^\nu \rho^{\nu *}, \tag{2.9}$$

where the superscript $*$ denotes an intrinsic variable. However, the partial and intrinsic pressure can be related by any functional relation, so long as (2.4) is not violated.

2.2. *The particle-size segregation model*

As the particles avalanche downslope and rearrange themselves during the segregation process, there are small changes in the local volume fraction of the interstitial fluid. For simplicity, the theory presented here assumes that these variations are small enough to be neglected and that the volume fraction of granular material, and hence the volume fraction of the background fluid, is constant

$$\Phi^g = \text{const} \quad \Rightarrow \quad \Phi^a = \text{const}. \tag{2.10}$$

The large and small particles are assumed to have the same constant intrinsic density, ρ^{g*}, while the passive fluid is assumed to have a constant density, ρ^{a*}, whose value is

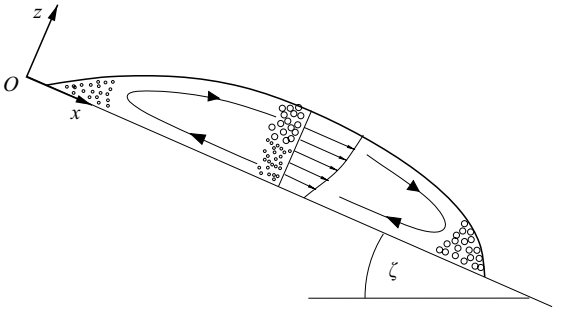

FIGURE 2. A diagram showing the coordinate system Oxz with the x-axis pointing down a chute, which is inclined at an angle ζ to the horizontal. The y-axis is into the plane of the paper and the z-axis is normal to the slope. Segregation causes inverse grading to develop in the centre of the avalanche and velocity shear then transports the large grains to the front and the fines to the rear.

in general different to that of the particles

$$\rho^{l*} = \rho^{s*} = \rho^{g*} = \text{const}, \qquad \rho^{a*} = \text{const}. \tag{2.11}$$

These assumptions imply that the bulk density is constant

$$\rho = \Phi^g \rho^{g*} + \Phi^a \rho^{a*} = \text{const}, \tag{2.12}$$

which is a reasonable first approximation in many granular free-surface flows (e.g. Savage & Hutter 1989). The second equation in (2.11) also implies that the fluid velocity field is incompressible $\nabla \cdot \boldsymbol{u}^a = 0$.

A coordinate system $Oxyz$ shown in figure 2 is defined with the x-axis pointing down a chute inclined an an angle ζ to the horizontal, the y-axis pointing across the chute and z-axis being the upward pointing normal. The velocity $\boldsymbol{u}^v$ has components (u^v, v^v, w^v) in the downslope, cross-slope and normal directions. Assuming that the normal acceleration terms are negligible the bulk momentum balance, obtained by summing (2.2) over all constituents, reduces to

$$\frac{\partial p}{\partial z} = -\rho g \cos\zeta, \tag{2.13}$$

in the normal direction, where g is the gravitational acceleration. Since the right-hand side of (2.13) is constant, the bulk momentum balance may be integrated through the avalanche depth h, subject to the boundary condition that the pressure is atmospheric at the free surface, $p(h) = p_{\text{atm}}$, to show that the bulk pressure is lithostatic

$$p = p_{\text{atm}} + \rho g (h - z) \cos\zeta. \tag{2.14}$$

The partial and intrinsic fluid pressures are assumed to be related by a linear volume fraction scaling, which is often used in mixture theory (e.g. Truesdell 1984; Morland 1992)

$$p^a = \Phi^a p^{a*}. \tag{2.15}$$

In order for the normal component of the fluid momentum equation (2.2) to reduce to a hydrostatic balance the interaction drag between the fluid and the grains must be (e.g. Morland 1992; Coussy, Dormieux & Detournay 1998)

$$\boldsymbol{\beta}^a = p^{a*} \nabla \Phi^a. \tag{2.16}$$

Physically this implies that fluid and the particles interact through interfacial pressure forces, but drag due to their relative motion is neglected. Substituting (2.15) and (2.16) into the normal component of (2.2) and assuming that the normal acceleration is negligible implies

$$\frac{\partial p^{a^*}}{\partial z} = -\rho^{a^*} g \cos\zeta. \tag{2.17}$$

This may also be integrated through the avalanche depth h, subject to the boundary condition that the pressure is atmospheric at the free surface, to show that the intrinsic fluid pore pressure is hydrostatic

$$p^{a^*} = p_{\rm atm} + \rho^{a^*} g(h - z)\cos\zeta. \tag{2.18}$$

The fluid pressure is transmitted through the entire matrix by surface pressure interaction forces. It follows that the remaining overburden pressure due to particle–particle contacts

$$p^{g^*} = p - p^{a^*}, \tag{2.19}$$

and using (2.14) and (2.18)

$$p^{g^*} = (\rho - \rho^{a^*}) g(h - z)\cos\zeta. \tag{2.20}$$

The key idea behind the segregation model is that while the small particles are falling through the matrix they support less of the overburden pressure p^{g^*} than the large particles, which must carry proportionately more of the load. The partial pressure in the grains therefore consists of a pressure due to the surrounding fluid, plus a share of the overburden pressure. Thus we propose that

$$p^{\mu} = \Phi^{\mu} p^{a^*} + f^{\mu} p^{g^*}, \qquad \mu = l, s, \tag{2.21}$$

where the factor f^{μ} determines the relative proportion of the overburden carried by constituents $\mu = l, s$. Specific forms for these factors have been proposed by Gray & Thornton (2005) and will be discussed in detail later, but the pressure sum (2.4) requires that $f^l + f^s = 1$. The second key assumption in the model is that the particles experience interparticle friction as they percolate past one another. A direct analogy with percolation of fluids through a porous matrix suggests a linear rate-dependent drag (e.g. Morland 1992; Coussy *et al.* 1998). We postulate mixture interaction terms of the form

$$\boldsymbol{\beta}^{\mu} = p^{a^*} \nabla \Phi^{\mu} + p^{g^*} \nabla f^{\mu} - \rho^{\mu} c(\boldsymbol{u}^{\mu} - \boldsymbol{u}), \qquad \mu = l, s, \tag{2.22}$$

where c is a dimensional constant and the barycentric granular velocity

$$\boldsymbol{u} = \phi^l \boldsymbol{u}^l + \phi^s \boldsymbol{u}^s. \tag{2.23}$$

The first term on the right-hand side of (2.22) is a reaction to the surface pressure forces induced by the fluid in (2.16). The second term is a grain–grain surface interaction force that ensures that the percolation is driven by an intrinsic gradient $-f^{\mu}\nabla p^{g^*}$. The third term provides the linear rate-dependent resistance to relative motion. Note that the internal interaction forces (2.16) and (2.22) and the pressure relations (2.15) and (2.21) have been constructed in such a way that they automatically satisfy the summation conditions (2.3) and (2.4).

Percolation velocities are typically of the same order of magnitude as the bulk normal velocity, which is much smaller than the downslope and cross-slope velocities in typical avalanche flows. The granular velocities in the downslope and cross-slope directions are therefore assumed to be equal to the bulk components

$$u^{\mu} = u, \qquad v^{\mu} = v, \qquad \mu = l, s. \tag{2.24}$$

An equation for the percolation velocities in the normal direction is obtained by substituting the partial/intrinsic pressure law (2.21), the interaction drag (2.22) and the pressure relations (2.14) and (2.18) into the normal component of (2.2) to give

$$\phi^{\mu}w^{\mu} = \phi^{\mu}w + (f^{\mu} - \phi^{\mu})(\hat{\rho}g/c)\cos\zeta, \qquad \mu = l, s, \tag{2.25}$$

where the relative density difference

$$\hat{\rho} = \frac{\rho^{g*} - \rho^{a*}}{\rho^{g*}}. \tag{2.26}$$

A comparison with the binary mixture theory of Gray & Thornton (2005) shows that the percolation equation (2.25) contains an additional factor $\hat{\rho}$ to account for the presence of the interstitial fluid. The simple two-constituent theory of Gray & Thornton (2005) can be recovered by assuming that the density of the interstitial fluid, ρ^{a*}, equals zero, so that $\hat{\rho} = 1$. Physically the addition of the passive fluid creates a buoyancy force on all the grains, which reduces the contact forces between them. In particular, if the density of the fluid is matched to the density of the particles to create a neutrally buoyant suspension with $\hat{\rho} = 0$, then (2.25) predicts that there will be no segregation due to kinetic sieving. This is in agreement with experimental observations of Vallance & Savage (2000), which will be discussed in § 2.4.

The final elements of the segregation model are the nonlinear pressure scalings, f^{μ}, which determine how the overburden pressure p^{g*} is shared between the large and small particles. The functions satisfy three constraints. They must sum to unity, $f^{l} + f^{s} = 1$, and when only one type of particle is present they must carry the entire overburden pressure, i.e.

$$\left.\begin{array}{lll} f^{l} = 1 & \text{when} & \phi^{s} = 0, \\ f^{s} = 1 & \text{when} & \phi^{s} = 1. \end{array}\right\} \tag{2.27}$$

Gray & Thornton (2005) proposed that

$$\left.\begin{array}{l} f^{l} = \phi^{l} + B\phi^{l}(1 - \phi^{l}), \\ f^{s} = \phi^{s} - B\phi^{s}(1 - \phi^{s}), \end{array}\right\} \tag{2.28}$$

where the non-dimensional factor $B > 0$ determines the magnitude of the pressure perturbation away from the hydrostatic. In general, B may be a function of a number of additional variables, and will lead to inverse grading provided that it does not change sign in the range $0 < \phi < 1$. Gray & Thornton (2005) showed that Savage & Lun's (1988) kinetic-sieving model can be recast in this form, with a function B that is dependent on six additional variables. In this paper the simplest possible segregation model is investigated in which B is constant.

The percolation velocities of the large and small particles relative to the bulk are obtained by substituting (2.28) into (2.25) to give

$$\left.\begin{array}{l} w^{l} - w = +q\phi^{s}, \\ w^{s} - w = -q\phi^{l}, \end{array}\right\} \tag{2.29}$$

where the mean segregation velocity

$$q = (B/c)\hat{\rho}g\cos\zeta. \tag{2.30}$$

An equation for the volume fraction of small particles is obtained by substituting (2.29) into the mass balance (2.1) and using (2.7) and (2.9) to give

$$\frac{\partial\phi^{s}}{\partial t} + \frac{\partial}{\partial x}(\phi^{s}u) + \frac{\partial}{\partial y}(\phi^{s}v) + \frac{\partial}{\partial z}(\phi^{s}w) - \frac{\partial}{\partial z}(q\phi^{s}\phi^{l}) = 0. \tag{2.31}$$

This equation describes the processes of advection and particle-size segregation by kinetic sieving and neglects other effects such as diffusive remixing and density differences between the particles. It does, however, allow for density differences between the particles and the interstitial fluid. For the vast majority of cases the fluid will be air and $\hat{\rho} > 0$. In this case the large particles move up and the small particles move down until they separate out to form sharply segregated inversely graded layers. A key prediction of this extended theory is that if the particles are neutrally buoyant, i.e. $\hat{\rho} = 0$, then no kinetic sieving will occur. Furthermore, if the relative density difference is negative, $\hat{\rho} < 0$, the particles are buoyant, the direction is segregation is reversed and *normally graded* layers are formed. It should be noted that the sharp segregation predicted in this paper ignores the effects of diffusive remixing, which smooths out the sharp interfaces into a continuous transitions.

2.3. *The non-dimensional segregation equation*

It is anticipated that this theory will be used in conjunction with existing avalanche models to compute segregation in shallow granular free-surface flows. The models all compute the avalanche thickness h and the bulk velocity $\boldsymbol{u}$ and fall into three basic categories: simple shallow-water-type avalanche theories of Grigorian *et al.* (1967), Kulikovskii & Eglit (1973), Eglit (1983) and Gray *et al.* (2003); Mohr–Coulomb models of Savage & Hutter (1989) and Gray *et al.* (1999); and debris-flow models of Iverson (1997) and Iverson & Denlinger (2001) that incorporate fluid in the pore space. These theories all assume that the granular material is incompressible, with a lithostatic pressure distribution through the avalanche depth, which is consistent with the model presented here. In addition, they assume that typical avalanche lengths L are much bigger than typical thicknesses H and that the flows are gravity driven. This gives rise to the scalings

$$x = L\tilde{x}, \quad z = H\tilde{z}, \quad (u, v, w) = \sqrt{Lg}\,(\tilde{u}, \tilde{v}, \varepsilon\tilde{w}), \quad t = \sqrt{L/g}\,\tilde{t}, \tag{2.32}$$

where the aspect ratio $\varepsilon = H/L \ll 1$ and the non-dimensional variables are denoted by tildes. Typically percolation velocities are of the same order of magnitude as normal velocities in the avalanche, so the segregation velocity can be scaled as

$$q = \varepsilon\sqrt{Lg}\,\tilde{q}. \tag{2.33}$$

Substituting these scalings into (2.31), and dropping the tildes on the avalanche variables and the superscript s for simplicity, the non-dimensional segregation equation for the small particles becomes

$$\frac{\partial \phi}{\partial t} + \frac{\partial}{\partial x}(\phi u) + \frac{\partial}{\partial y}(\phi v) + \frac{\partial}{\partial z}(\phi w) - S_r \frac{\partial}{\partial z}(\phi(1-\phi)) = 0, \tag{2.34}$$

where the non-dimensional segregation number

$$S_r = \frac{LB\hat{\rho}g\cos\zeta}{cH\sqrt{gL}}. \tag{2.35}$$

Exact steady-state and two-dimensional time-dependent solutions to (2.34) have been constructed by Gray & Thornton (2005) for a constant-thickness steady uniform flow with a homogeneously mixed inflow condition. These show the formation of two concentration shocks that separate pure phases of large and small particles from a region still at the inflow concentration. Eventually the two shocks meet at a distance $1/S_r$ downstream and a third slope-parallel shock is formed, which separates the large particles from the small particles beneath to form a fully separated inversely graded

Liquid	Viscosity (cP)	Fluid density ρ^{a*} (g cm^{-3})	Relative density difference $\hat{\rho}$
Water	1.0	1.00	0.59
Water–ethanol mixture	3.7	0.94	0.62

TABLE 1. Summary of the properties of the different interstitial fluids used in the liquid–particle segregation experiments of Vallance & Savage (2000).

layer. A larger segregation number therefore implies a shorter distance for complete segregation to occur.

2.4. *Comparison with experiments*

Gray & Thornton (2005) showed that their exact solutions were in good agreement with the dry granular segregation experiments of Savage & Lun (1988) and Vallance & Savage (2000). Experiments with liquid–particle mixtures were also performed by Vallance & Savage (2000). They used a bi-disperse mixture of 1.44 mm large and 0.99 mm small glass particles of density $\rho^{g*} = 2.49\,\mathrm{g\,cm^{-3}}$, which were mixed in a water and a water–ethanol mixture, whose properties are summarized in table 1. The mass flux was regulated to generate a steady uniform flow of depth 0.9 to 1.5 cm on slopes ranging from 22° to 12.3°, which developed a uniform solids fraction once the initial flow front had propagated through the system. Splits were taken at three different levels in the flows to determine the degree of segregation at four downstream stations. They found that segregation took place, but that it was not as "dramatic as in the dry granular flows" and they surmised that the presence of a viscous fluid inhibited kinetic sieving. Curiously, they found that the segregation was slightly weaker in water than in the water–ethanol mixture, which 3.7 times more viscous. This contradicted their initial hypothesis that it was due to viscosity and they suggested that this might instead be due to the density contrast between the particles and the fluid. The theory presented in this paper confirms the latter hypothesis. From Gray & Thornton (2005) the segregation distance $x_p = 1/S_r$. It follows that the ratio of the segregation distances

$$\frac{x_{p1}}{x_{p2}} = \frac{S_{r2}}{S_{r1}} = \frac{\hat{\rho}_2}{\hat{\rho}_1} \simeq 1.04, \tag{2.36}$$

where the subscript 1 is used for water and the subscript 2 for the water–ethanol mixture. Hence, the segregation distance in water is 4 % longer than in the slightly less dense water–ethanol mixture, as observed. The buoyancy induced by the interstitial fluid is therefore more important than the effects of viscosity in these high-solids-fraction experiments. Vallance & Savage (2000) also investigated segregation in neutrally buoyant fluids. However, they concluded that "there is very little evidence of size segregation in flows where the fluid and the particles have exactly the same density", as the downstream concentrations of small particles stayed at the inflow concentration to within the level of accuracy of the experiments. This is also consistent with the model derived here. When the particles and the fluid have the same density, the relative density difference $\hat{\rho} = 0$ and the segregation length therefore tends to infinity. As far as the authors are aware no experiments have been performed with buoyant particles to date, but the theory predicts that the direction of segregation will reverse to create normally graded layers.

3. Steady-state solutions for normally graded initial conditions

Gray & Thornton's (2005) exact solutions for the segregation of a homogeneously mixed inflow were motivated by the experiments and approximate solutions of Savage & Lun (1988). In practice, it is quite difficult to generate a homogeneous inflow, and an alternative inflow configuration in which the particles are normally graded, i.e. with the small particles on top of the large particles, is now considered. This problem is of fundamental interest because the inflowing particles are unstably stratified and must adjust into a stable configuration.

3.1. *General solution for arbitrary positive velocity fields*

Using the uniform flow depth H to scale the height and the inflow velocity magnitude U to scale the velocity in (2.32), we may assume without loss of generality that the avalanche is of unit thickness and the integral of the velocity over the depth is equal to unity, i.e. $\int_0^1 u(z)\,\mathrm{d}z = 1$. Assuming that the particle-size distribution has reached steady state and substituting the velocity components

$$u = u(z) \geqslant 0, \quad v = 0, \quad w = 0, \quad \text{in} \quad 0 \leqslant z \leqslant 1, \quad x \geqslant 0, \tag{3.1}$$

the non-dimensional segregation equation (2.34) reduces to

$$\frac{\partial}{\partial x}(\phi u) - S_r \frac{\partial}{\partial z}(\phi(1-\phi)) = 0. \tag{3.2}$$

The inflow concentration is assumed to be normally graded with a pure phase of small particles lying above a pure phase of large particles

$$\phi(0, z) = \begin{cases} 1, & z_r \leqslant z \leqslant 1, \\ 0, & 0 \leqslant z < z_r, \end{cases} \tag{3.3}$$

where z_r is the height of the sharp interface at $x = 0$. In addition, no particles are allowed through the free surface and base of the flow, which implies that the flux

$$\mathscr{F} = -S_r\phi(1-\phi) = 0 \quad \text{at} \quad z = 0, 1. \tag{3.4}$$

This is satisfied when either $\phi = 0$ or $\phi = 1$ at the free surface and base of the avalanche.

Expanding the derivatives, the segregation equation (3.2) can be written as

$$u(z)\frac{\partial \phi}{\partial x} + S_r(2\phi - 1)\frac{\partial \phi}{\partial z} = 0, \tag{3.5}$$

which is a simple first-order quasi-linear equation. The small particle concentration ϕ is equal to a constant ϕ_λ on each characteristic curve given by

$$u(z)\frac{\mathrm{d}z}{\mathrm{d}x} = S_r(2\phi_\lambda - 1). \tag{3.6}$$

By defining a depth-integrated velocity coordinate

$$\psi = \int_0^z u(z')\,\mathrm{d}z', \tag{3.7}$$

equation (3.6) can be integrated for a general velocity field, to give the straight line characteristic

$$\psi = S_r(2\phi_\lambda - 1)(x - x_\lambda) + \psi_\lambda, \tag{3.8}$$

in the mapped variables, where $(x_\lambda, \psi_\lambda)$ is its starting position. Note that the velocity has been scaled so that the mapped coordinate $\psi = 1$ at the free surface $z = 1$. The

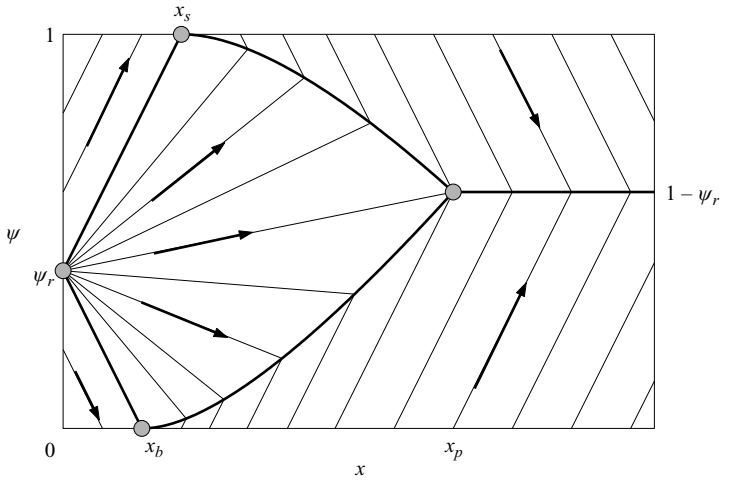

FIGURE 3. The steady-state solution in depth-integrated velocity coordinates (x, ψ). The inflow concentration jump is located at $(0, \psi_r)$ and the bulk flow is from left to right. The characteristics are shown as straight thin lines and the arrows show their direction of propagation. A rarefaction fan is centred at the discontinuity and a series of characteristics radiate away from it. The front marking the first small particles that propagate downwards is indicated by the downward bold characteristic emanating from the fan. This reaches the base at a distance $x_b = \psi_r/S_r$ downstream and a curved (bold) shock wave is generated that separates the expansion fan from the pure phase of small particles that gather beneath. A similar situation occurs at the top boundary, where the large particles first reach the surface at $x_s = (1-\psi_r)/S_r$ and a curved shock is generated that separates the pure phase of large particles from the expansion fan. At a distance x_p downstream the two shocks meet and a third slope-parallel shock at height $1-\psi_r$ is formed, creating a completely segregated inversely graded layer.

mapping between the physical and depth-integrated coordinates can be constructed once the velocity is prescribed, and is well-defined provided $u \geqslant 0$ and any points with zero velocity are isolated. As a result the depth-integrated velocity transformation allows solutions to be constructed for a whole class of velocity fields. Specific cases will be investigated further in § 3.3.

Figure 3 shows how the characteristics propagate downstream from the inflow at $x = 0$. The characteristics carry information into the domain and are not to be confused with the particle paths, which are computed in § 3.2 and are illustrated in figure 4. Above the inflow discontinuity $\psi_r = \psi(z_r)$ the particles are all small and the characteristics propagate upwards with gradient S_r, while below the discontinuity, where the particles are all large, the characteristics propagate downwards with gradient $-S_r$. The void in between has to be filled with information. The only way to do this with boundary data is to construct a series of characteristics centred at $(0, \psi_r)$ with concentrations varying between 0 and 1, so that the whole of the space is filled as shown in figure 3. A centred rarefaction fan is therefore formed at $(0, \psi_r)$ within which the concentration

$$\phi = \frac{1}{2}\left(1 + \frac{\psi - \psi_r}{S_r x}\right), \quad |\psi - \psi_r| < S_r x. \tag{3.9}$$

The $\phi_\lambda = 0$ characteristic emanating from the fan propagates down until it reaches the base of the flow at $x_b = \psi_r/S_r$. Physically this characteristic represents the front between a region of purely large particles and the first small particles that

propagate downwards. Within the avalanche a downward motion of small particles automatically implies that there is a corresponding upward flux of large particles by (2.29). However, at the lower boundary, there are no more large particles available and the flux condition (3.4) implies that the small particles separate out into a pure phase. This concentration shock then propagates upwards into the domain as more and more particles separate out.

Gray & Thornton (2005) showed that the segregation equation (3.2) implies that a shock $z = s(x)$ must satisfy the jump condition

$$[\![\phi u s' + S_r \phi(1-\phi)]\!] = 0 \tag{3.10}$$

where $s' = \mathrm{d}s/\mathrm{d}x$ and the jump bracket $[\![\gamma]\!] = \gamma^+ - \gamma^-$ is the difference of the enclosed quantity on the forward '+' and rearward '−' sides of the shock. The shock condition (3.10) can be rearranged to give

$$u\frac{\mathrm{d}s}{\mathrm{d}x} = S_r(\phi^+ + \phi^- - 1), \tag{3.11}$$

which is an ordinary differential equation for the height of the shock. This has a similar structure to the characteristic equation (3.6) and the depth-integrated coordinate transformation (3.7) implies that mapped shock satisfies

$$\frac{\mathrm{d}\psi}{\mathrm{d}x} = S_r(\phi^+ + \phi^- - 1). \tag{3.12}$$

The shock ψ_1, that forms when the lead characteristic $\phi_\lambda = 0$ reaches the base, has a pure phase of small particles on the forward side, $\phi^+ = 1$, and the expansion fan (3.9) on the rearward side. Substituting these into (3.12) implies

$$\frac{\mathrm{d}\psi_1}{\mathrm{d}x} = \frac{S_r}{2}\left(1 + \frac{\psi_1 - \psi_r}{S_r x}\right), \tag{3.13}$$

which is linear and can be integrated subject to the initial condition that $\psi_1 = 0$ at $x = \psi_r/S_r$ to give the height of the bottom shock

$$\psi_1 = \psi_r + S_r x - 2\sqrt{S_r \psi_r x}. \tag{3.14}$$

A similar situation develops on the upper side of the expansion fan. The $\phi_\lambda = 1$ characteristic marks the front of large particles that propagate upwards into the pure phase of small particles entering from the inflow. This reaches the free surface $\psi = 1$ at $x_s = (1-\psi_r)/S_r$ and a shock ψ_2 is formed between a pure phase of large particles on the forward side, $\phi^+ = 0$, and the expansion region (3.9) on the rearward side. The shock condition (3.12) yields a linear ordinary differential equation which can be integrated to give

$$\psi_2 = \psi_r - S_r x + 2\sqrt{S_r(1-\psi_r)x}. \tag{3.15}$$

The lower shock (3.14) increases in height with downstream distance x, while the upper shock decreases in height. The two shocks meet at

$$x_p = \frac{1}{S_r}\left(\sqrt{\psi_r} + \sqrt{1-\psi_r}\right)^2, \qquad \psi_p = 1 - \psi_r, \tag{3.16}$$

and a third shock ψ_3 is formed between the large and small particles. In this case the jump condition (3.12) reduces to $\mathrm{d}\psi/\mathrm{d}x = 0$, so that the shock

$$\psi_3 = \psi_p, \qquad x \geqslant x_p, \tag{3.17}$$

is parallel to the downstream coordinate. The point x_p determines the downstream location at which complete segregation first occurs. It is proportional to $1/S_r$, which, like the solutions of Gray & Thornton (2005), show that inversely graded layers form at shorter downstream distances when the segregation number S_r is larger. The segregation distance also depends on the height of the inflow discontinuity, z_r, which is qualitatively different to the homogeneous inflow case, where the distance for complete segregation was independent of the initial concentration. These pure segregation solutions are a good leading-order approximation to flows with weak diffusive remixing, replacing rapid smooth transitions with sharp concentration jumps.

3.2. *Particle paths*

To understand the solution in § 3.1 it is instructive to know how the large and small grains move through the fan. The particle path of constituent ν is given by solving

$$\frac{\mathrm{d}x}{\mathrm{d}t} = u^{\nu}, \quad \frac{\mathrm{d}y}{\mathrm{d}t} = v^{\nu}, \quad \frac{\mathrm{d}z}{\mathrm{d}t} = w^{\nu}, \quad \nu = l, s, \tag{3.18}$$

where the velocities are given by (2.24) and (2.29). For steady uniform two-dimensional flows, where the bulk velocity is given by (3.1), these equations can be solved by rewriting them as $u\,\mathrm{d}z/\mathrm{d}x = w^{\nu}$ and using the depth-integrated coordinate transformation (3.7) to yield an ordinary differential equation for the mapped particle path

$$\frac{\mathrm{d}\psi}{\mathrm{d}x} = w^{\nu}, \quad \nu = l, s. \tag{3.19}$$

For the large particles $w^l = S_r\phi$. It follows that if a large particle enters the chute at $x = 0$ with height $\psi_{lo} \in [0, \psi_r]$, with local concentration $\phi = 0$, then the particle moves downstream at its initial height ψ_{lo} until it intersects with the expansion fan at

$$x_{lo} = (\psi_r - \psi_{lo})/S_r. \tag{3.20}$$

Within the expansion fan the concentration is given by (3.9) and the equation for the particle path reduces to

$$\frac{\mathrm{d}\psi_l}{\mathrm{d}x} = \frac{S_r}{2}\left(1 + \frac{\psi_l - \psi_r}{S_r x}\right), \tag{3.21}$$

which is linear and is easily solved subject to the boundary condition that $\psi_l = \psi_{lo}$ at $x = x_{lo}$ to give the large-particle path

$$\psi_l = \psi_r + S_r x - 2\sqrt{S_r x_{lo}}\sqrt{S_r x}. \tag{3.22}$$

This hits the top shock at

$$x_{le} = (\sqrt{1 - \psi_r} + \sqrt{S_r x_{lo}})^2/S_r, \quad \psi_{le} = 1 - S_r x_{lo}, \tag{3.23}$$

where it enters the pure phase and moves downstream at constant height ψ_{le}. A series of particle paths for different initial starting heights is shown in figure 4 using solid curves. Large particles move downstream at constant height until they reach the fan, where they move up through the avalanche while being swept downstream. Eventually they cross the top shock and then move downslope at constant height again.

The small-particle paths can be computed analogously by using the normal velocity of the small particles $w^s = -S_r(1 - \phi)$ in (3.19). The small particles start at $x = 0$ at a height $\psi_{so} \in [\psi_r, 1]$ and at concentration $\phi = 1$. Equation (3.19) implies that they

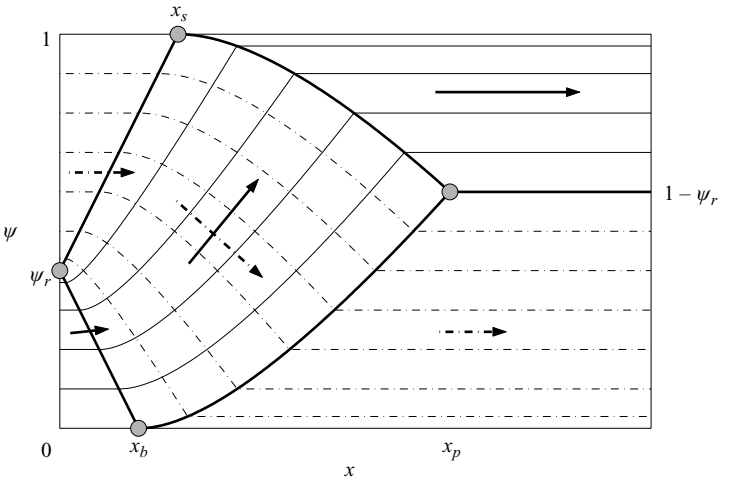

FIGURE 4. The steady-state particle paths for the large (solid lines) and small (dot-dash lines) grains in mapped coordinates. The arrows show the direction of flow.

move downslope at constant height ψ_{so} until they intersect with the fan at

$$x_{so} = (\psi_{so} - \psi_r)/S_r. \tag{3.24}$$

Within the fan (3.19) implies that the small particles drop down along the paths

$$\psi_s = \psi_r - S_r x + 2\sqrt{S_r x_{so}}\sqrt{S_r x}, \tag{3.25}$$

until they meet the bottom shock at

$$x_{se} = (\sqrt{\psi_r} + \sqrt{S_r x_{so}})/S_r, \quad \psi_{se} = S_r x_{so}, \tag{3.26}$$

and subsequently move downstream at constant height ψ_{se}. The small-particle paths are also illustrated in figure 4 using dot-dash lines. The large and small particles cross over within the expansion fan, but otherwise move downslope at constant height.

3.3. *Physical solutions*

Granular free-surface flows exhibit a range of velocity profiles dependent on the macroscopic roughness of the topography the avalanche is sliding over. Observations of geophysical-scale flows (Dent *et al.* 1998; Keller, Ito & Nishimura 1998) over fairly 'smooth' surfaces show that there is a well-defined slip layer at the base of the flow and weak shear above. Consequently, many avalanche models assume a 'plug-flow' regime. In contrast, small-scale experiments on macroscopically bumpy slopes show that there is significant shear through the avalanche depth and the mean velocity scales with the thickness to the $3/2$ power (Vallance 1994; Pouliquen 1999). The leading-order behaviour of many of these velocity fields is captured by a linear velocity profile of the form

$$u = \alpha + 2(1-\alpha)z, \quad 0 \leqslant \alpha \leqslant 1, \tag{3.27}$$

which gives plug flow for $\alpha = 1$, simple shear for $\alpha = 0$ and a combination of shear and basal slip for parameter values in between. With this velocity field the depth-integrated velocity mapping (3.7) implies

$$\psi = \alpha z + (1-\alpha)z^2, \tag{3.28}$$

which has the advantage that it can be easily inverted, i.e.

$$z = \begin{cases} \psi, & \alpha = 1, \\ \dfrac{-\alpha + \sqrt{\alpha^2 + 4(1-\alpha)\psi}}{2(1-\alpha)}, & \alpha \neq 1, \end{cases} \tag{3.29}$$

to give the position of the shocks, expansions and characteristics in physical space. The solutions are illustrated for three values of α and two values of z_r in figure 5(a–f) for $S_r = 1$. A contour scale is used to help identify regions of high concentrations of small particles (light greys) and coarse grains (dark greys). Figure 5(a, b) corresponds to plug flow. In this case the physical and depth-integrated coordinates are identical, $\psi = z$, so the fan is bounded by straight lines and the upper and lower curved concentration shocks have linear and square-root dependence as defined in (3.15) and (3.14). The point x_p where the two shocks meet, and the grains separate out into stratified inversely graded layers, is dependent on the height of the inflow discontinuity z_r. Equation (3.16) implies $x_p = 2$ for $z_r = 1/2$, while for $z_r = 0.7$ the shocks meet slightly earlier at $x_p = 1.91$.

Figure 5(c, d) shows the solutions for linear shear and translation with $\alpha = 1/2$, which requires the full quadratic mapping (3.28). The characteristics in the expansion fan are now curved, rather than straight. This is because as the small particles percolate down through the matrix their downslope velocity becomes progressively less, even though the percolation velocity at a given concentration remains constant by (2.29). Another key feature is that the thickness of the bottom inflowing layer of large particles is much thinner than the surface outflowing one. This is a direct result of the velocity shear. In the upper layers of the flow the velocity is much faster than in the lower layers and so the same mass flux can be achieved with a much thinner layer of material. The segregation length x_p, where the two shock meet, is in almost the same position for both $z_r = 0.5$ and 0.7. For simple shear, $\alpha = 0$ (figure 5 e, f), the reverse mapping (3.29) reduces to $z = \sqrt{x}$. The lower characteristic, which marks the first small particles percolating downwards and emanates from the fan, has an infinite gradient at $z = 0$, which is caused by the zero velocity at the base of the avalanche. In addition, the lower shock now has a concave instead of convex profile and the layer of rapidly moving large particles far downstream is even thinner than for linear shear and translation. Interestingly, the segregation length is now longer for $z_r = 0.7$ than for $z_r = 0.5$, at $x_p = 1.99$ and $x_p = 1.86$, reversing the order found in plug flow. Figure 6 shows how the segregation length $S_r x_p$ varies as a function of α and z_r. The maximum segregation length $S_r x_p$ is equal to 2 and this is attained when $\psi_r = 1/2$, or, equivalently, when $\alpha = (1/2 - z_r^2)/(z_r - z_r^2)$ as shown by the dot-dash line. The segregation distance is strongly dependent of z_r and only weakly dependent on α.

Experiments show that on low-inclination macroscopically bumpy slopes a steady uniform flow develops in which the velocity scales with thickness to the 3/2 power (Vallance 1994; Pouliquen 1999). Recently Silbert *et al.* (2003) have used molecular dynamics simulations to investigate these flows and showed that Bagnold's (1954) grain inertia regime, in which the shear stress is proportional to the square of the strain rate, $\sigma_{xz} = A^2(\partial u/\partial z)^2$, had the right constitutive properties. From this they were able to derive an expression for the downslope velocity profile through the avalanche depth, which is in excellent agreement with their numerical simulations. Scaling the thickness on the flow depth and their velocity on the magnitude $U = 2(\rho g \sin\zeta)^{1/2} h^{3/2}/(5A)$

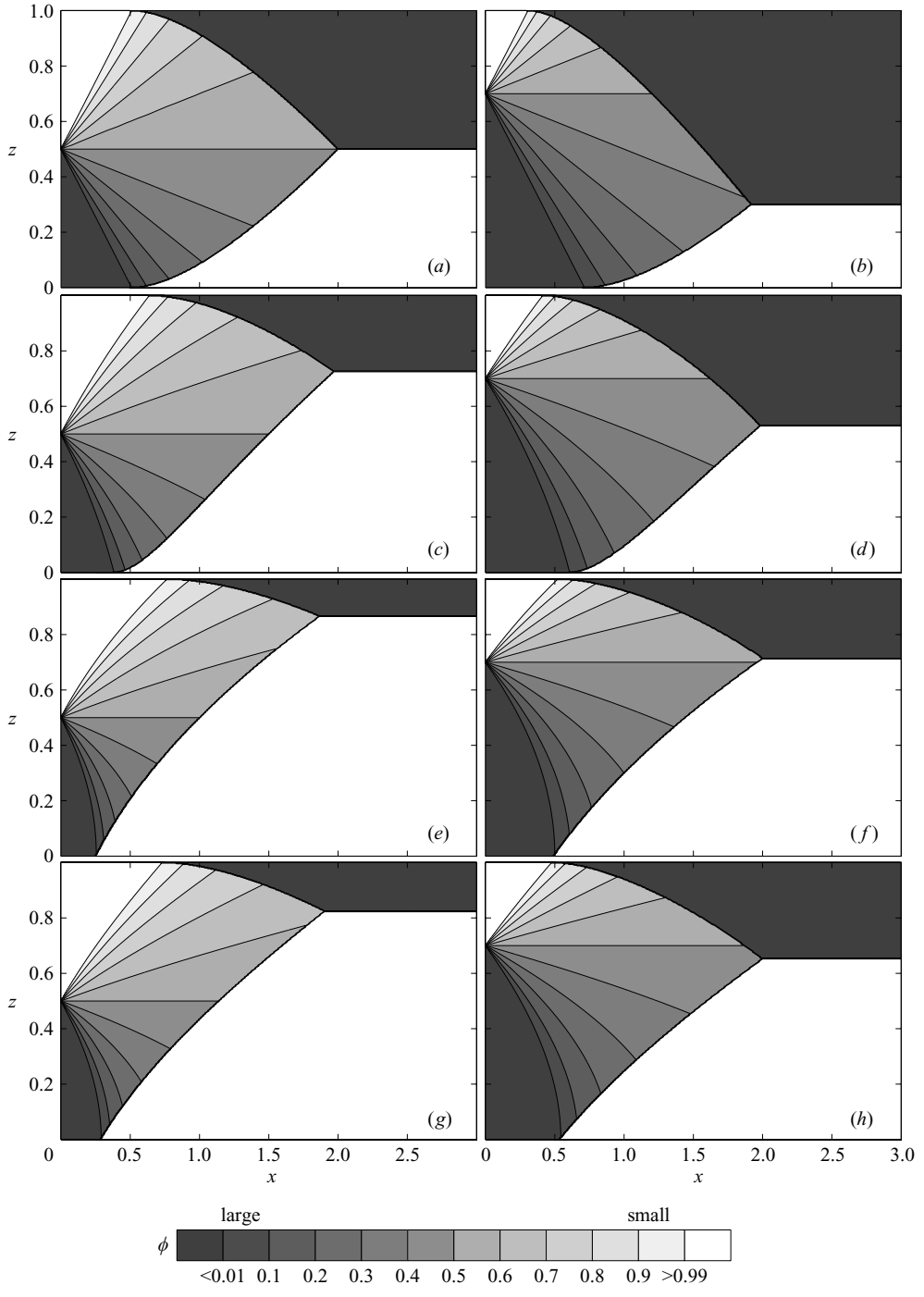

FIGURE 5. Steady-state solutions for the concentration of small particles ϕ are shown as a function of the downslope coordinate x and avalanche depth z for $S_r = 1$. The concentration is shown using a contour scale with lighter greys corresponding to larger concentrations of small particles. The bulk flow is from left to right with panels (a, b) corresponding to plug flow ($\alpha = 1$), panels (c, d) to linear shear and translation ($\alpha = 1/2$), panels (e, f) to simple shear ($\alpha = 0$) and panels (g, h) to $u = 5[1 - (1 - z)^{3/2}]/3$. The solution is plotted for $z_r = 0.5$ (left, a, c, e, g) and $z_r = 0.7$ (right, b, d, f, h).

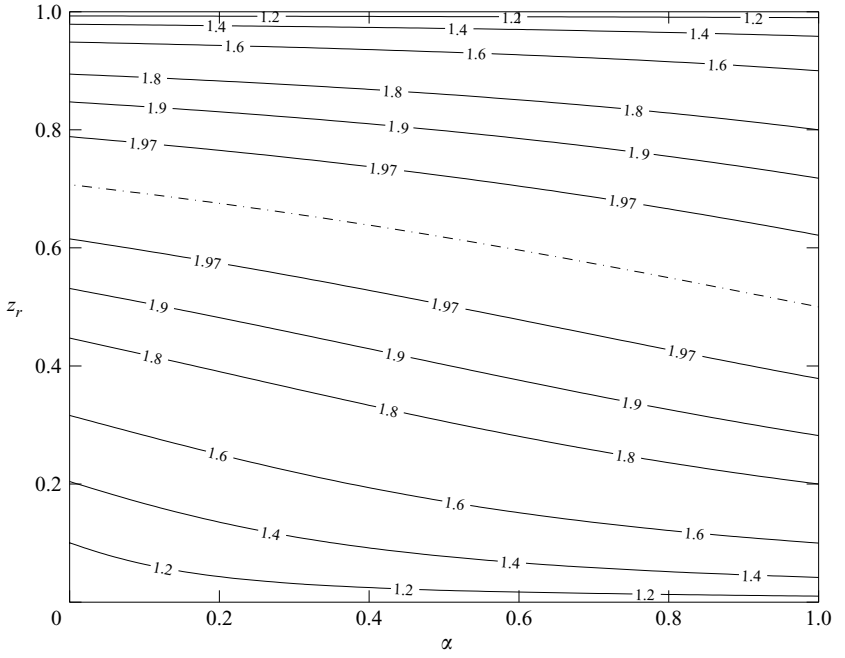

FIGURE 6. A contour plot of the segregation distance $S_r x_p$ as a function of the linear velocity profile parameter α and the initial discontinuity height z_r. The dot-dash line shows the points where the maximum value of $S_r x_p = 2$ is attained.

(Gray & Thornton 2005) the non-dimensional velocity profile reduces to

$$u = \tfrac{5}{3}\left[1 - (1-z)^{3/2}\right], \tag{3.30}$$

which yields the mapping

$$\psi = \tfrac{5}{3}z - \tfrac{2}{3}\left[1 - (1-z)^{5/2}\right]. \tag{3.31}$$

A direct reverse mapping to get $z = z(\psi)$ is not possible, so explicit solutions for the shocks and expansions cannot be generated. It is, however, very easy to contour the solution, by setting up a regular (x, z) grid, working out the value of ψ for each point and setting the value of ϕ based on which region of mapped space (x, ψ) the point lies. The solutions are plotted in figure 5(g,h). In fact, they look very similar to those for simple shear, as the velocity is zero at the base of the flow so the lower shock also has a concave profile. The final thickness of the inversely graded layer of large particles is, however, slightly thicker than for simple shear.

4. Time-dependent solutions for uniform plug flows

Considerable insight into the nature of two-dimensional time-dependent solutions can be obtained by considering the case of plug flow, which admits a class of particularly simple solutions. These are based on the physical observation that, because there is no shear, each material column of grains segregates independently of all the others. Without loss of generality the plug velocity u_0 may be assumed to equal unity by virtue of the scalings (2.32). Gray & Thornton (2005) showed that the transformation

$$t' = t - t_c, \quad \xi = x - u_0 t, \quad z' = z, \tag{4.1}$$

with time-shift parameter t_c, implies that the segregation equation (2.34) reduces to

$$\frac{\partial \phi}{\partial t'} - S_r \frac{\partial}{\partial z}(\phi(1-\phi)) = 0, \tag{4.2}$$

in the moving frame when the cross-slope derivatives are zero. This has exactly the same structure as the steady-state segregation equation (3.2) except that $u\partial/\partial x$ is now replaced by $\partial/\partial t'$. The solutions are therefore exactly equivalent to those given by (3.9), (3.14), (3.15), (3.16) and (3.17) with ψ replaced by z and x by t'. The concentration within the expansion fan is therefore

$$\phi = \frac{1}{2}\left(1 + \frac{z - z_r}{S_r t'}\right), \quad |z - z_r| < S_r t', \quad z_1 < z < z_2, \tag{4.3}$$

where the shocks

$$\left.\begin{array}{ll} z_1 = z_r + S_r t' - 2\sqrt{S_r z_r t'}, & t' < t_p, \\ z_2 = z_r - S_r t' + 2\sqrt{S_r(1-z_r)t'}, & t' < t_p, \\ z_3 = 1 - z_r, & t' \geqslant t_p, \end{array}\right\} \tag{4.4}$$

and the triple-point

$$t_p = \frac{1}{S_r}\left(\sqrt{z_r} + \sqrt{1-z_r}\right)^2. \tag{4.5}$$

This time-dependent solution for the evolution of the concentration in a column of material moving downstream with speed u_0 is effectively illustrated in figure 5(a,b) except that x-axis must now be replaced by the t'-axis.

Each column can be uniquely labelled by its position $\xi = x$ at $t = 0$ and a two-dimensional time-dependent solution can be constructed by considering a series of columns with different time shifts $t_c = t_c(\xi)$ and discontinuity heights $z_r = z_r(\xi)$. To give an example of this, we now construct the solution to a problem in which the material in $x \geqslant 0$ is initially normally graded with the initial discontinuity height $z_r = 1/2$ and any material that enters the chute at $x = 0$ is also normally graded with the same height z_r, i.e.

$$\left.\begin{array}{lll} t_c = 0, & z_r = 0.5, & \text{for} \quad \xi \geqslant 0, \\ t_c = -\xi/u_0, & z_r = 0.5, & \text{for} \quad \xi < 0. \end{array}\right\} \tag{4.6}$$

The solution generated by (4.1) and (4.3)–(4.6) is illustrated in figure 7. It consists of two parts. For $\xi \geqslant 0$ a spatially uniform time-dependent expansion wave develops and shock waves are subsequently generated when the fronts reach the surface and base of the flow. These then propagate into the domain before they meet to form a spatially and temporally uniform third concentration shock separating an inversely graded layer of large particles from the fines beneath. For the points that enter the chute at time $t_c = -\xi/u_0$ the transformation (4.1) implies that

$$t' = x/u_0 \quad \text{for} \quad \xi < 0. \tag{4.7}$$

When this is substituted into the column solution (4.3)–(4.5) we see that the temporal evolution in moving columns entering the chute is equivalent to a steady-state solution in a fixed frame of reference. A *transition line* $\xi = 0$ therefore moves downstream at speed u_0 and separates the time-dependent solution from the steady-state solution behind. At time $t = 2$ the upper and lower shocks meet in the time-dependent region to form an inversely graded layer and there is no further change in the

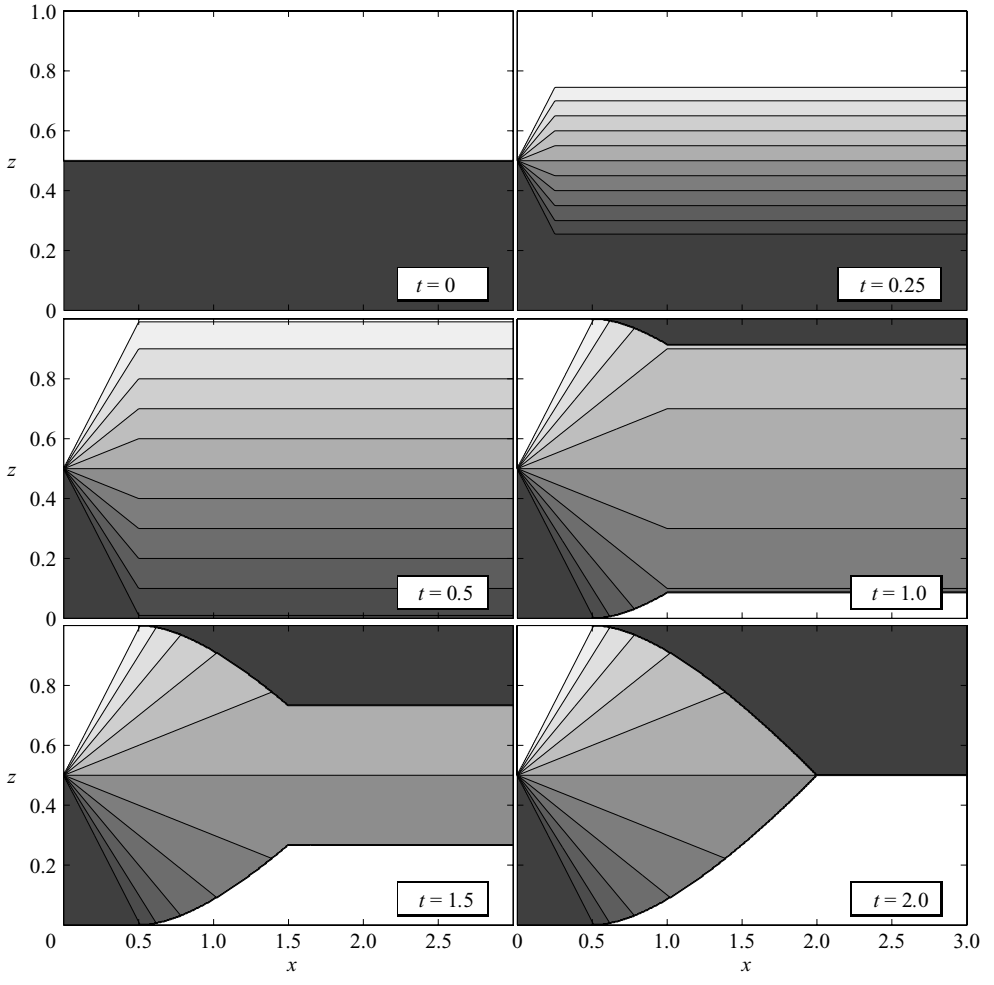

FIGURE 7. The exact plug-flow solution for the concentration of small particles ϕ is illustrated at a sequence of time-steps using the same contour scale as in figure 5. Initially the flow is normally graded and normally graded material is fed in at $x = 0$ and flows downstream from left to right. The solution consists of a time-dependent spatially uniform part that is separated by a transition line moving downstream at speed u_0 from a steady-state region behind. The parameter $z_r = 1/2$ for all columns and the segregation number $S_r = 1$.

solution. In plug flow the solution therefore attains a global steady state in finite time.

5. Numerical solutions for time-dependent flows with shear

Solutions to more complex problems can be computed by solving the segregation equation (2.34) with a high-resolution shock-capturing method. Gray & Thornton (2005) developed a TVD Lax Friedrichs scheme for (2.34), using Godunov-type operator splitting (e.g. LeVeque 2002), that was based on the general algorithms of Yee (1989) and Tóth & Odstrcil (1996). This method has been tested against the exact plug-flow solution of § 4 and is now used to compute solutions to some complex segregation problems with shear.

5.1. *Chute initially normally graded*

Suppose that initially the granular material is normally graded with all the small particles overlying the coarse grains

$$\phi(0, x, z) = \begin{cases} 1, & z_r \leqslant z \leqslant 1, \\ 0, & 0 \leqslant z \leqslant z_r, \end{cases} \qquad x \geqslant 0, \tag{5.1}$$

as in the exact solution for plug flow. This is solved subject to the boundary conditions that the inflow discontinuity also lies at the same height z_r and that there is no normal flux of small particles out of the free surface or the base of the avalanche (3.4). The solution for a velocity field given by $\alpha = 1/2$, which has both linear shear and basal slip, is shown in figure 8. The numerical solution has many similarities with both the two-dimensional time-dependent plug-flow solution and the steady-state solutions of § 3. As the initial distribution is independent of the downslope coordinate x the time-dependent part of the solution, which evolves from the initial conditions, is in fact identical to plug flow, while the material that flows onto the chute creates a steady-state region, which is identical to the solution in figure 5(*c*). Between the two regions there is a complex transition. For $t < 1/2$, as the fan propagates towards the boundaries, the transition starts parallel to the z-axis and slowly tips over to the right in response to the shear. Once the upper and lower shocks are generated the transition widens into a relaxation zone as the solution matches the time-dependent and steady-state shocks, which, as opposed to plug flow, now lie at different heights. At $t = 2$ the upper and lower shocks meet and a third shock is produced, which lies at height $z_3 = 1/2$ in the initially uniform region. As the transition propagates further downslope the two steady-state shocks meet just before $t = 2.5$ to produce a steady-state shock that lies at $z_3 = (\sqrt{6} - 1)/2$. The third shock has a fairly linear transition region between these two regions, which is advected downstream and out of the domain by $t = 3.5$. The solution therefore reaches a local steady state, but the mismatch persists and eventually breaks far downstream.

5.2. *Chute initially filled with large particles*

The evolution towards the local steady state can be markedly different. Consider now the alternative case in which the chute is initially filled with large particles

$$\phi(0, x, z) = 0, \quad 0 < z < 1, \quad x \geqslant 0, \tag{5.2}$$

subject to the same boundary conditions (3.3) and (3.4) as before. For plug flow the solution would look similar to figure 7 except that the time-dependent region would be replaced by a constant uniform state of large particles. When there is a velocity gradient, the small particles are progressively sheared across the top of a region of large grains beneath and immediately start to percolate down through the matrix as shown in figure 9. By $t = 0.5$ a complex transition region develops between the steady-state solution to the left and the constant uniform state of large particles to the right, which appears to consist of an additional unsteady shock and an expansion fan. Once the lower characteristic reaches the base a pure region of small (white) particles separates out at the bottom ($t = 1$) and a lower finite-length unsteady shock develops. This grows in size and eventually cuts off the unsteady transition expansion between $t = 2.5$ and 2.6, to leave the steady-state fan behind. The unsteady expansion is eroded and disappears by $t = 3$ to leave a concentration jump between the large particles above and the fines beneath. This is swept downstream and eventually breaks far downslope, but a local steady state is attained by $t = 3.5$.

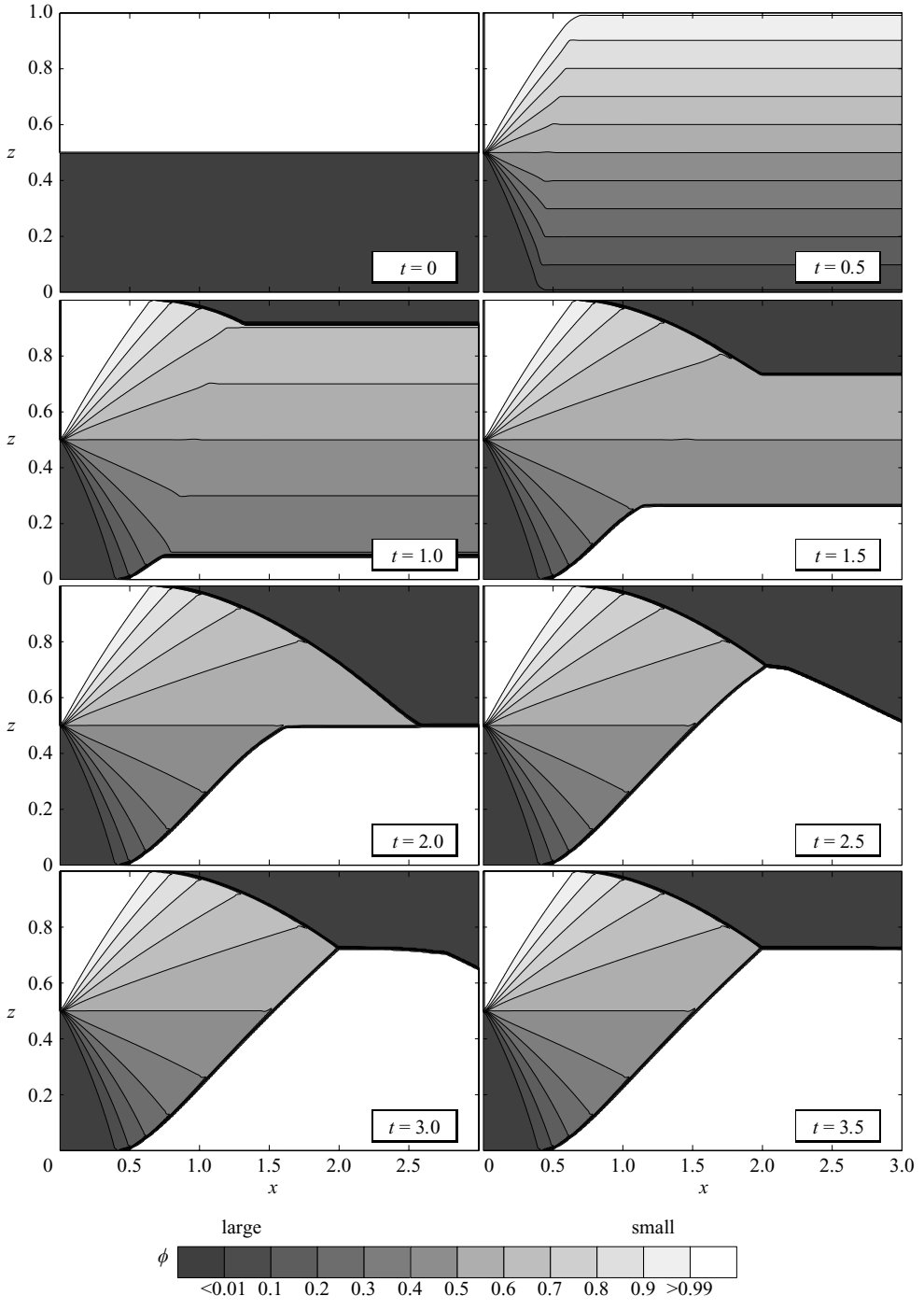

FIGURE 8. The numerical solution for the concentration of small particles ϕ is shown using a contour scale at a series of time-steps for a chute initially filled with normally graded material with the small particles overlying the large ones. A linear velocity profile with basal slip ($\alpha = 1/2$) transports the material downslope from left to right and normally graded material is fed onto the chute at $x = 0$ to replenish the avalanche. The discontinuity height $z_r = 1/2$ and the segregation number $S_r = 1$.

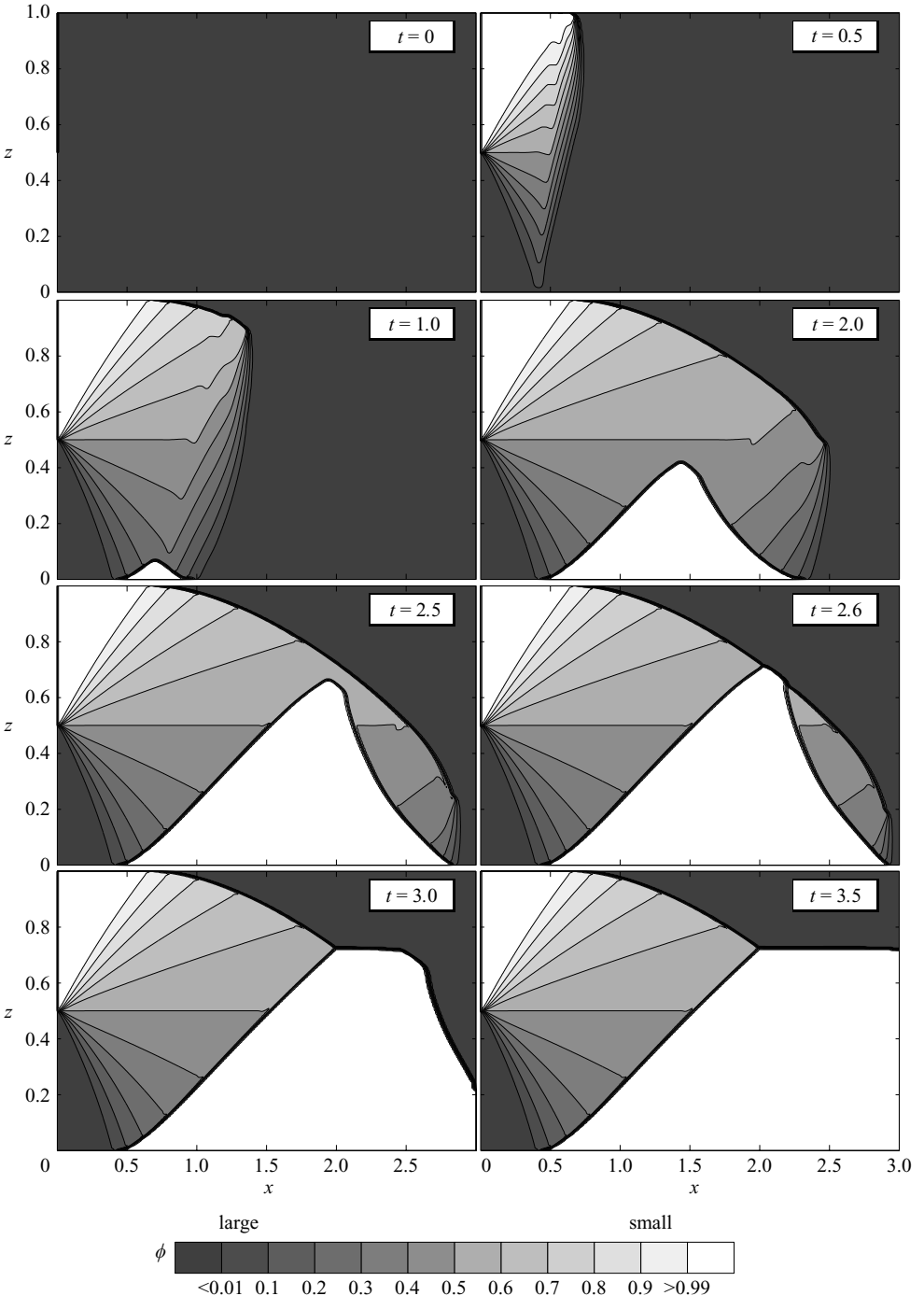

FIGURE 9. The numerical solution for the concentration of small particles ϕ is shown using a contour scale at a series of time-steps for a chute that was initially filled with large particles. A linear velocity profile with basal slip ($\alpha = 1/2$) transports the material downslope from left to right and normally graded material is fed onto the chute at $x = 0$ to replenish the avalanche. The discontinuity height $z_r = 1/2$ and the segregation number $S_r = 1$.

6. Discussion and conclusions

The framework of mixture theory has been used to derive a model for particle-size segregation by kinetic sieving in shallow gravity-driven granular free-surface flows. The material is composed of large particles, small particles and a passive interstitial fluid that allows buoyancy effects to be incorporated into the final segregation equation (2.34). This represents a significant extension of the simple two-phase theory of Gray & Thornton (2005). Exact steady-state solutions have been constructed for a discontinuous normally graded inflow condition with general steady uniform velocity fields. These show the formation of expansion fans, concentration shocks and inversely graded completely segregated layers sufficiently far downstream. The distance for complete segregation to occur is inversely proportional to the segregation number S_r and is dependent on the inflow discontinuity height z_r. This is in marked contrast to the homogeneous inflow solutions of Gray & Thornton (2005), which were only dependent on S_r. As the density of the interstitial fluid is increased, the relative density difference $\hat{\rho}$ decreases, so S_r decreases and complete segregation occurs further downstream. If the density of the fluid and the grains match, then segregation by kinetic sieving is inhibited altogether. This is in agreement with the experiments of Vallance & Savage (2000), but it should be noted that segregation in other more energetic systems may occur in the absence of gravity due to spatial gradients in the energy of the granular velocity fluctuations (e.g. Louge *et al.* 2000; Jenkins & Yoon 2001). If the relative density difference $\hat{\rho}$ changes sign, so that the particles are buoyant, the direction of segregation is reversed and normally graded layers will be formed sufficiently far downstream. The solutions constructed in this paper ignore the effects of diffusive remixing, which tend to smooth out sharp concentration gradients and jumps. The solutions are nevertheless a very good leading-order approximation for segregation in flows with weak diffusive remixing.

A high-resolution shock-capturing method (Gray & Thornton 2005) has been used to compute the evolution of the small-particle concentration with strong shear in two space dimensions and time. Many of the flow features can be explained with the insight gained from some simple exact solutions for plug flow that exploit the decoupling of material columns in the absence of downslope velocity gradients through the avalanche depth. Essentially the solutions consist of a downstream region, where the uniformity of the initial conditions implies that the solution is exactly that predicted by plug flow, and a steady-state upstream region, which are separated by an evolving transition zone that propagates downslope with increasing time. The dynamics of the transition regions are extremely complex, with the development of unsteady propagating shocks and expansion fans. However, the system is suitably robust to suggest that the segregation equation (2.34) may be coupled to existing models for dry granular free-surface flows (e.g. Grigorian *et al.* 1967; Kulikovskii & Eglit 1973; Eglit 1983; Savage & Hutter 1989; Gray *et al.* 1999; Gray *et al.* 2003) to compute the development of the particle-size distribution and allow feedback onto the flow. In particular, the inclusion of a passive fluid now allows the model to be incorporated into water-saturated debris-flow models such as those of Iverson (1997) and Iverson & Denlinger (2001).

This research was generously supported by an EPSRC Doctoral Training Account, an EPSRC Advanced Research Fellowship (GR/S50052/01 & GR/S50069/01) and a Royal Society grant (22919).

REFERENCES

Bagnold, R. A. 1954 Experiments on a gravity-free dispersion of large spheres in a Newtonian fluid under shear. *Proc. R. Soc. Lond.* A **255**, 49–63.

Bridgwater, J. 1976 Fundamental powder mixing mechanisms. *Powder Tech.* **15**, 215–236.

Calder, E. S., Sparks, R. S. J. & Gardeweg, M. C. 2000 Erosion, transport and segregation of pumice and lithic clasts in pyroclastic flows inferred from ignimbrite at Lascar Volcano, Chile. *J. Volcan. Geotherm. Res.* **104**, 201–235.

Cooke, M. H., Stephens, D. J. & Bridgwater, J. 1976 Powder mixing – a literature survey. *Powder Tech.* **15**, 1–20.

Coussy, O., Dormieux, L. & Detournay, E. 1998 From mixture theory to Biot's approach for porous media. *Intl J. Solids Structures* **35**, 4619–4635.

Davidson, J. F., Scott, D. M., Bird, P. A., Herbert, O., Powell, A. A. & Ramsey, H. V. M. 2000 Granular motion in a rotary kiln: the transition from avalanching to rolling. *KONA Powder and Particle* **18**, 149–155.

Dent, J. D., Burrel, K. J., Schmidt, D. S., Louge, M. Y., Adams, E. E. & Jazbutis, T. G. 1998 Density, velocity and friction measurements in a dry-snow avalanche. *Annal. Glac.* **26**, 247–252.

Dolgunin, V. N. & Ukolov, A. A. 1995 Segregation modelling of particle rapid gravity flow. *Powder Tech.* **83**, 95–103.

Eglit, M. E. 1983 Some mathematical models of snow avalanches. In *Advances in Mechanics and the Flow of Granular Materials* (ed. M. Shahinpoor), vol. 2, pp. 577–588. Clausthal-Zellerfeld and Gulf Publishing Company.

Gray, J. M. N. T. 2001 Granular flow in partially filled slowly rotating drums. *J. Fluid Mech.* **441**, 1–29.

Gray, J. M. N. T., Tai, Y.-C. & Noelle, S. 2003 Shock waves, dead-zones and particle-free regions in rapid granular free surface flows. *J. Fluid Mech.* **491**, 161–181.

Gray, J. M. N. T. & Thornton, A. R. 2005 A theory for particle size segregation in shallow granular free-surface flows. *Proc. R. Soc. Lond.* A **461**, 1447–1473.

Gray, J. M. N. T., Wieland, M. & Hutter, K. 1999 Free surface flow of cohesionless granular avalanches over complex basal topography. *Proc. R. Soc. Lond.* A **455**, 1841–1874.

Grigorian, S. S., Eglit, M. E. & Lakimov, Lu. L. 1967 New statement and solution of the problem of the motion of snow avalanche. In *Snow, Avalanches & Glaciers. Tr. Vysokogornogo Geofizich Inst.* 12.

Hill, K. M. & Kakalios, J. 1995 Reversible axial segregation of rotating granular media. *Phys. Rev.* E **52**, 4393–4400.

Hill, K. M., Kharkar, D. V., Gilchrist, J. F., McCarthy, J. J. & Ottino, J. M. 1999 Segregation-driven organization in chaotic granular flows. *Proc. Natl Acad. Sci. USA* **96**, 11689–12210.

Iverson, R. M. 1997 The physics of debris flows. *Rev. Geophys.* **35**, 245–296.

Iverson, R. M. 2003 The debris-flow rheology myth. In *Debris-flow Hazards Mitigation: Mechanics, Prediction and Assessment* (ed. D. Rickenmann & C. L. Chen), pp. 303–314. Millpress, Rotterdam.

Iverson, R. M. & Denlinger, R. P. 2001 Flow of variably fluidized granular masses across three-dimensional terrain 1. Coulomb mixture theory. *J. Geophys. Res.* **106** (B1), 553–566.

Iverson, R. M. & Vallance, J. W. 2001 New views of granular mass flows. *Geology* **29**, 115–118.

Jenkins, J. T. 1998 Particle segregation in collisional flows of inelastic spheres. In *Physics of Dry Granular Media* (ed. H. J. Herrmann, J.-P. Hovi & S. Luding), pp. 645–658. NATO ASI series, Kluwer.

Jenkins, J. T. & Mancini, F. 1987 Balance laws and constitutive relations for plane flows of a dense, binary mixture of smooth nearly elastic, circular disks. *J. Appl. Mech.* **54**, 27–34.

Jenkins, J. T. & Yoon, D. 2001 Segregation in binary mixtures under gravity. *Phys. Rev. Lett.* **88**, 194301-4.

Johanson, J. R. 1978 Particle segregation ··· and what to do about it. *Chem. Engng*, May 8, 183–188.

Keller, S., Ito, Y. & Nishimura, K. 1998 Measurements of the vertical velocity distribution in ping pong ball avalanches. *Annal. Glac.* **26**, 259–264.

Kulikovskii, A. G. & Eglit, M. E. 1973 Two-dimensional problem of the motion of a snow avalanche along a slope with smoothly changing properties. *Prikl. Mat. Mekh.* **37**(5), 837–848. (English transl. *J. Appl. Math. Mech.* **37**(5), 792–803.)

LeVeque, R. J. 2002 *Finite Volume Methods for Hyperbolic Problems*. Cambridge University Press.

Louge, M. Y., Jenkins, J. T., Reeves, A. & Keast, S. 2000 Microgravity segregation in collisional granular shearing flows. In *IUTAM Symp. on Segregation in Granular Materials* (ed. A. D. Rosato & D. L. Blackmore), pp. 103–112. Kluwer.

Metcalfe, G., Shinbrot, T., McCarthy, J. J. & Ottino, J. M. 1995 Avalanche mixing of granular solids. *Nature* **374**, 39–41.

Middleton, G. V. & Hampton, M. A. 1976 Subaqueous sediment transport and deposition by sediment gravity flows. In *Marine Sediment Transport and Environmental Management* (ed. D. J. Stanley & D. J. P. Swift), pp. 197–218. Wiley.

Morland, L. W. 1992 Flow of viscous fluids through a porous deformable matrix. *Surveys in Geophysics* **13**, 209–268.

Pouliquen, O. 1999 Scaling laws in granular flows down inclined planes. *Phys. Fluids* **11**, 542–548.

Pouliquen, O., Delour, J. & Savage, S. B. 1997 Fingering in granular flows. *Nature* **386**, 816–817.

Pouliquen, O. & Vallance, J. W. 1999 Segregation induced instabilities of granular fronts. *Chaos* **9**, 621–630.

Savage, S. B. & Hutter, K. 1989 The motion of a finite mass of granular material down a rough incline. *J. Fluid Mech.* **199**, 177–215.

Savage, S. B. & Lun, C. K. K. 1988 Particle size segregation in inclined chute flow of dry cohesionless granular solids. *J. Fluid Mech.* **189**, 311–335.

Shinbrot, T., Alexander, A. & Muzzio, F. J. 1999 Spontaneous chaotic granular mixing. *Nature* **397**, 675.

Silbert, L. E., Ertas, D., Grest, G. S., Haley, T. C., Levine, D. & Plimpton, S. J. 2001 Granular flow down an inclined plane: Bagnold scaling and rheology. *Phys. Rev.* E **64**, 051302.

Spurling, R. J., Davidson, J. F. & Scott, D. M. 2001 The transient response of granular flows in an inclined rotating cylinder. *Trans. Inst. Chem. Engng* **79**, 51–61.

Staniforth, J. N. 1982 Determination and handling of total mixes in pharmaceutical systems. Powder Tech. **33**, 147–159.

Tóth, G. & Odstrcil, D. 1996 Comparison of flux corrected transport and total variational diminishing numerical schemes for hydrodynamic and magnetohydrodynamic problems. *J. Comput. Phys.* **128**, 82–100.

Truesdell, C. 1984 *Rational Thermodynamics*. Springer.

Vallance, J. W. 1994 Experimental and field studies related to the behaviour granular mass flows and the characteristics of their deposits. PhD thesis Michigan Technological University.

Vallance, J. W. 2000 Lahars. In *Encyclopedia of Volcanoes*, pp. 601–616. Academic.

Vallance, J. W. & Savage, S. B. 2000 Particle segregation in granular flows down chutes. In *IUTAM Symp. on Segregation in Granular Materials* (ed. A. D. Rosato & D. L. Blackmore), pp. 31–51. Kluwer.

Williams, J. C. 1968 The mixing of dry powders. *Powder Tech.* **2**, 13–20.

Yee, H. C. 1989 A class of high-resolution explicit and implicit shock-capturing methods. *NASA TM* 101088.

Zik, O., Levine, D., Lipson, S. G., Shtrikman, S. & Stavans, J. 1994 Rotationally induced segregation of granular materials. *Phys. Rev. Lett.* **73**, 644–647.